

Performance-defining properties of Nb₃Sn coating in SRF cavities

Y Trenikhina¹, S Posen¹ , A Romanenko¹, M Sardela², J-M Zuo² , D L Hall³ and M Liepe³

¹ Fermi National Accelerator Laboratory, Batavia, IL 60510, United States of America

² Materials Science and Engineering Department, University of Illinois, Urbana IL 61801, United States of America

³ Cornell Laboratory for Accelerator-Based Sciences and Education, Ithaca, NY 14853, United States of America

E-mail: yuliatr@fnal.gov

Received 30 June 2017, revised 29 August 2017

Accepted for publication 27 October 2017

Published 22 November 2017



Abstract

Nb₃Sn has potential to become the material of choice for fabrication of SRF cavities. The higher critical temperature of Nb₃Sn potentially allows for an increased operational temperature in SRF cavities, which could enable a simplification of the cryogenic system, leading to significant cost reduction. We present extended characterization of a Nb₃Sn coated Nb cavity prepared at Cornell University. Using a combination of thermometry during cavity RF measurements, and structural and analytical characterization of the cavity cutouts, we discovered Nb₃Sn coating flaws in regions that exhibit significant heating during the RF testing. Results of extended comparison of cavity cutouts with different dissipation profiles not only indicate the cause of significant *Q* degradation but also establish figures of merit for material qualities in relation to the quality of SRF performance.

Keywords: Nb₃Sn, SRF materials, films, microscopy

(Some figures may appear in colour only in the online journal)

1. Introduction

Superconducting radio frequency (SRF) cavities are the technology of choice for most modern particle accelerators [1, 2]. Traditionally, SRF cavities are made of bulk niobium, which has superconducting critical temperature of $T_c = 9.2$ K. Growing demand for higher SRF cavity performance at higher accelerating gradients has brought traditional niobium close to its theoretical limits. Nb₃Sn alloy is one of the primary alternative materials for SRF cavity production. Being a type II superconductor with maximum T_c of 18 K and predicted superheating field of 400 mT [3], Nb₃Sn may offer improvements in both cryogenic efficiency and maximum accelerating field.

A physical vapor deposition apparatus constructed at Cornell University for the production of Nb₃Sn coatings on Nb cavities [4, 5] has produced 1.3 GHz 1-cell cavities that do not exhibit the strong *Q*-slope degradation—i.e. increase in surface resistance with accelerating gradient—that had been observed previously, notably in experiments at U Wuppertal [6]. Despite encouraging development of Nb₃Sn technology for the SRF field, systematic understanding is absent for the cause of quench fields which have been observed in the 14–17 MV m⁻¹ range. Furthermore, while these highest performing modern Nb₃Sn-coated cavities exhibit a near-constant quality factor with increasing accelerating gradient, systematic understanding is also absent for the cause of the *Q*-slope that has been observed in other cavities [6, 7].

The major challenge is to understand why the expected theoretical level of Nb₃Sn performance is still out of reach. In order to understand and overcome cavity performance limitations, fundamental intrinsic properties of the Nb₃Sn



Original content from this work may be used under the terms of the [Creative Commons Attribution 3.0 licence](#). Any further distribution of this work must maintain attribution to the author(s) and the title of the work, journal citation and DOI.

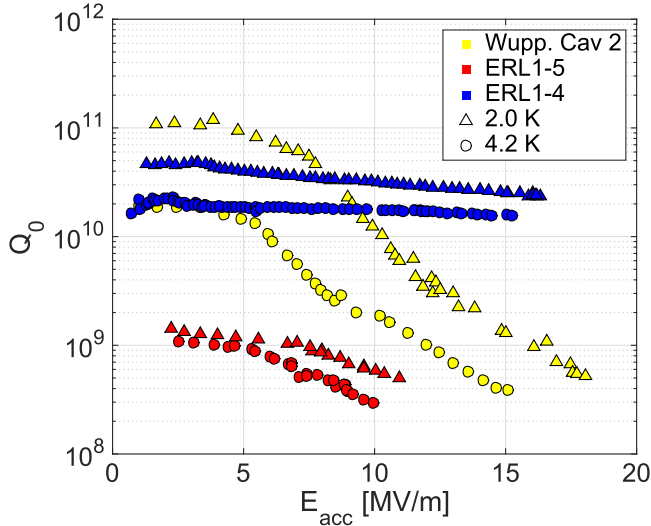


Figure 1. Q versus E curves for different Nb₃Sn-coated cavities. Wupp. Cav2 was coated at U Wuppertal and tested at Jefferson Lab in the late '90s [6]. ERL1-5 was the first cavity coated in the Cornell program, and cutouts from it are analyzed in this paper [8]. ERL1-4 was coated later in the Cornell program, with modified coating procedure, and did not exhibit the strong Q -slope [9].

coating need to be evaluated. While construction of Fermilab's Nb₃Sn coating facility was in progress [10], we initiated extended characterization of the first Nb₃Sn coated cavity (ERL1-5) from Cornell University. Though subsequent cavities coated at Cornell showed much higher quality factors [11], this 1.3G Hz single cell Nb₃Sn coated cavity exhibited a fairly poor (for Nb₃Sn) low-field Q_0 on the order of 10^9 at 4.2 K as well as Q -slope reminiscent of that observed previously at U Wuppertal (Wupp. Cav 2) [6], as shown in figure 1. ERL1-5 gives us an opportunity to study the type of Nb₃Sn surface features that cause cavity performance limitation, in particular degradation of the quality factor. In the next section, it will be shown that this cavity is especially suited for this study, as it has regions that dissipate strongly (hot spots), and others with minimal heating (cold spots).

This paper discusses structural and analytical characterization of Nb₃Sn coating in cavity cutouts with different dissipation characteristics. We use x-ray diffraction (XRD), scanning electron microscopy (SEM), transmission electron microscopy (TEM), Scanning TEM (STEM) and energy dispersive spectroscopy (EDS). Use of a temperature mapping system during the RF measurements of Nb₃Sn-coated Nb cavity enables us to directly relate properties of the coating to the local dissipation profiles. The use of multiple material characterization techniques provides complete insight into composition, homogeneity and structure of Nb₃Sn coating for SRF application.

2. Experimental methods

2.1. Identification of the cutout regions

The first cavity coated under Cornell's program [12], ERL1-5 demonstrated significantly degraded performance compared

to the cavities which had been Nb₃Sn-coated at Cornell afterwards. Temperature maps show significant heating that is mostly observed in one half-cell (figure 2). In addition, the visual appearance of the two half-cells seems to be different. Looking into the surfaces of the cavity visible from the beamtubes, one half-cell appears matte gray as expected, while the other appears shiny. Attempts to re-coat the same cavity resulted in similar appearance of the half-cells and similar quality of performance [8].

ERL1-5 is a 1.3 GHz single cell Nb cavity coated with Nb₃Sn at Cornell University [8] that has been RF characterized at Cornell in 2013 and at Fermilab in 2015 (figure 2). The half-cell with the unusually shiny appearance has large regions with far higher surface resistance than is observed in the other half-cell, according to temperature maps measured in 2013 at Cornell and at 2015 and Cornell and Fermilab. The intention of repeated measurement was to map out well the surface resistance of the cavity, so that the 'hot' and 'cold' regions could be identified with a high degree of confidence. Coupons located at these hot and cold spots were subsequently cut out from the cavity by an automated milling machine with pure water used as a lubricant. Cutouts were in a 1 cm diameter, circular shape. Two cutouts were chosen for the analysis. The spot marked as 'H4' on the temperature map, was taken from the shiny half-cell as representative of strongly dissipating region (referred as hot spot). 'C2' on the temperature map indicates the location of a non-dissipating cold spot taken from the matte half-cell (figure 2(c)). Figures 3(a) and (b) shows optical images of cold cutout (C2) and hot cutout (H4), respectively.

Direct comparison of the original H4 and C2 cutouts allows us to relate differences in the coating quality to the dissipation profiles. The ultimate goal of our work is not only to find out coating qualities which lead to the unsatisfactory performance but also to understand why poorly performing regions are produced during the coating process.

In addition to the hot and cold cutouts, two cutouts taken from the equator region of the cavity (referred as equator cutouts, E2 and E4) were characterized, as well as one Nb₃Sn coated flat Nb sample. The Nb₃Sn-coated flat sample was coated in the same experimental setup at Cornell University. Characterization of the flat Nb₃Sn-coated sample with different substrate geometry provides additional insight to the intrinsic properties of Nb₃Sn.

2.2. Characterization techniques

Cross-sectional TEM samples were prepared from Nb₃Sn-coated Nb cavity cutouts and extracted by focused ion beam (FIB) using a Helios 600 FEI instrument at the Materials Research Laboratory (MRL) at the University of Illinois at Urbana-Champaign (UIUC). A JEOL JEM 2100 LaB₆ thermionic gun TEM at MRL/UIUC was used for imaging and nano-area electron diffraction (NED). The beam size of approximately 100 nm was used to obtain NED patterns. A Pananalytical/Philips X'pert¹ Material Research Diffractometer at MRL/UIUC was used for XRD. The X'pert¹ system is a high-resolution XRD system which uses Cu k-alpha1 radiation

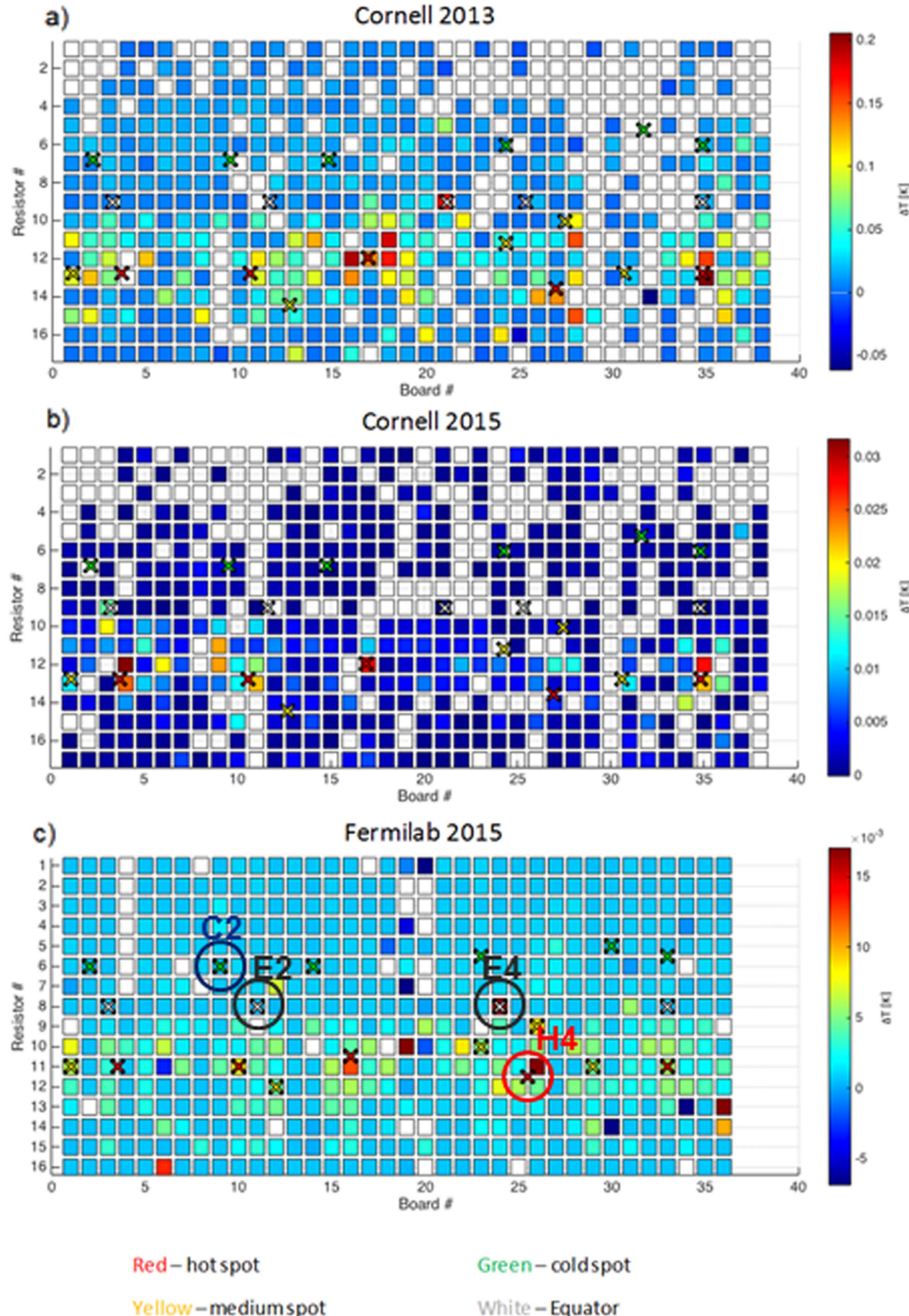


Figure 2. Temperature maps showing excessive heating in one half-cell (regions below resistor 9 on the Cornell T-map and below resistor 8 on the Fermilab T-map). First measurements were taken at Cornell in 2013 (a) then new studies were performed in 2015 at Cornell (b) and FNAL (c). Reproduced from <http://accelconf.web.cern.ch/AccelConf/SRF2015/papers/tupb049.pdf>. CC BY 3.0.

with a hybrid mirror (x-ray mirror and a two-reflection Ge monochromator) in the primary optics, and has a PIXcel line detector in the secondary optics. X'pert¹ resolution in the 2theta configuration is 0.01°.

A Hitachi HD2300 Dual EDS STEM at Northwestern University (NU) was used for STEM imaging and EDS

chemical analysis. STEM images were taken with a high angle annular dark field detector. EDS maps were measured with incident electron energy of 200 kV. Frame time was set to 10 s. Map resolution was set to 512 by 384 pixels. A Hitachi SU8030 SEM with cold field emission gun equipped with EDS silicon drift detector at NU was used for imaging

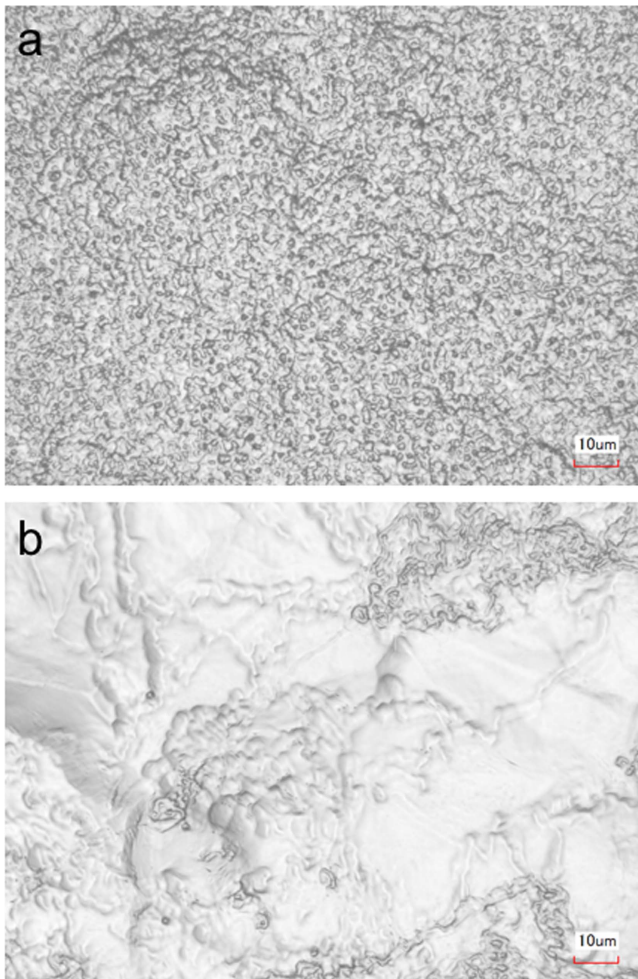


Figure 3. Images of (a) cold and (b) hot cutouts from optical microscope.

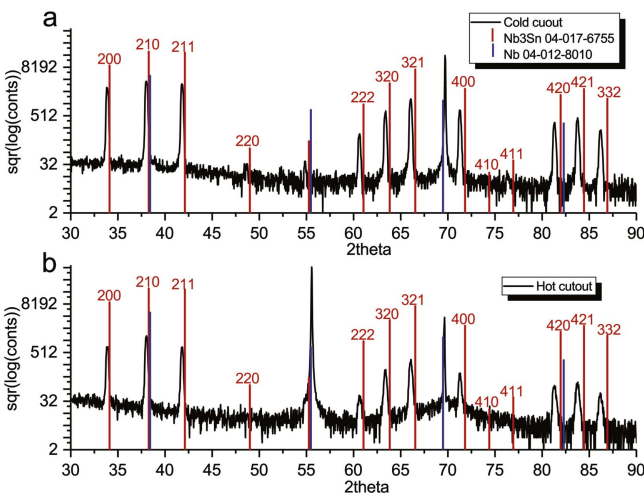


Figure 4. XRD in (a) cold and (b) hot cutouts. Red and blue markers indicate positions of the reference peaks for Nb_3Sn and Nb, respectively.

and EDS analytical characterization. A Hitachi S-3400N SEM equipped with Oxford WAVE wavelength-dispersive spectroscopy (WDS) system was used for WDS quantitative analysis. Integrated Oxford AZtec system on FEI Quanta field

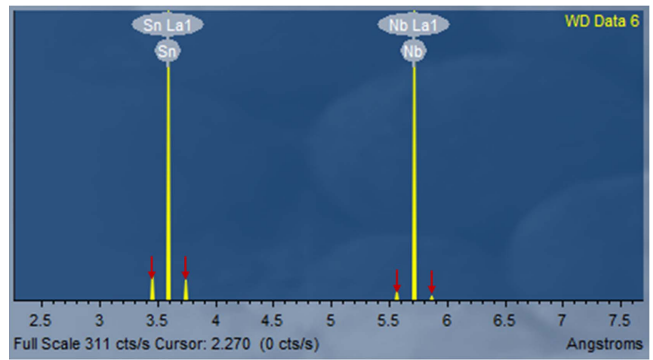


Figure 5. WDS spectrum in the cold cutout. Quantification based on La_{α_1} Nb and Sn peaks. Red arrows indicate the scanning range.

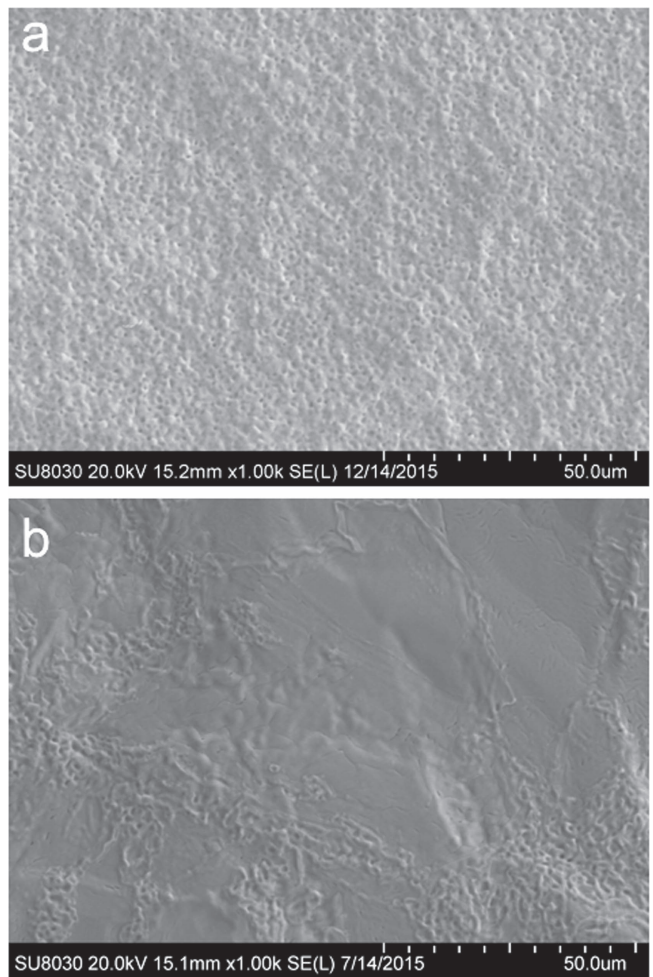


Figure 6. SEM images of (a) cold and (b) hot cutouts.

emission gun SEM at NU was used for EBSD and additional EDS.

3. Results and discussion

3.1. Structural evaluation

Structural characterization of ERL1-5 cavity cutouts was initiated in order to confirm the A15 Nb_3Sn structure of the

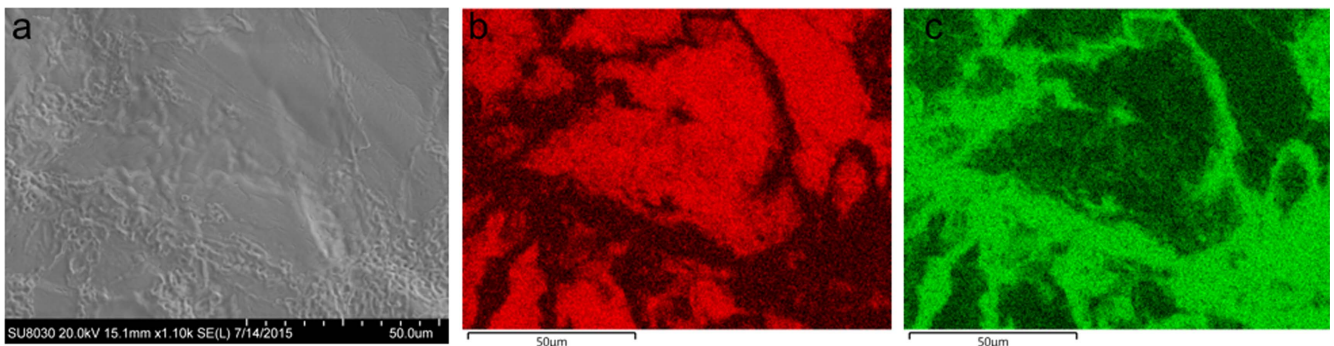


Figure 7. (a) SEM image of hot cutout with corresponding (b) Nb and (c) Sn maps at 20 kV.

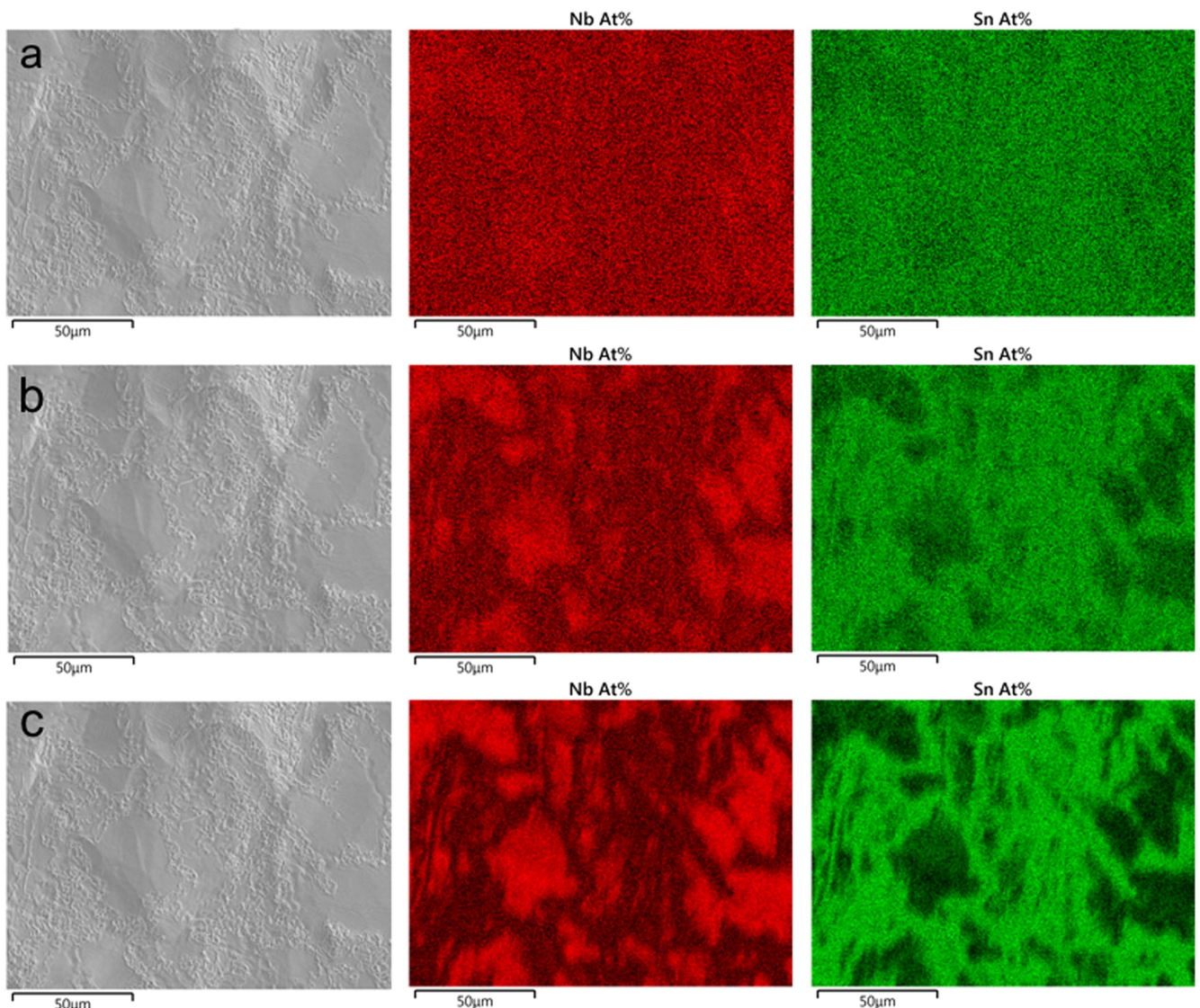


Figure 8. SEM images and EDS maps of Sn and Nb taken from the same spot on hot cutout at (a) 10 kV, (b) 15 kV, and (c) 20 kV. Reproduced from <http://accelconf.web.cern.ch/AccelConf/SRF2015/papers/tupb049.pdf>. CC BY 3.0.

coating and the absence of non-stoichiometric phases, such as Nb_6Sn_5 . XRD measurements showed A15 Nb_3Sn structure (PDF 04-012-8010) in both cold and hot cutouts. Figures 4(a) and (b) demonstrate data for the cold and hot cutout, respectively. Due to the relatively large probing depth of

XRD, signal from the Nb substrate is also present (PDF 04-012-8010). XRD confirmed the absence of non-A15 phases in the coating. The Lattice constant of Nb_3Sn was estimated from the peak fitting. The Lattice constant in the cold cutout was estimated to be $5.289 \pm 0.002 \text{ \AA}$. Lattice constant of

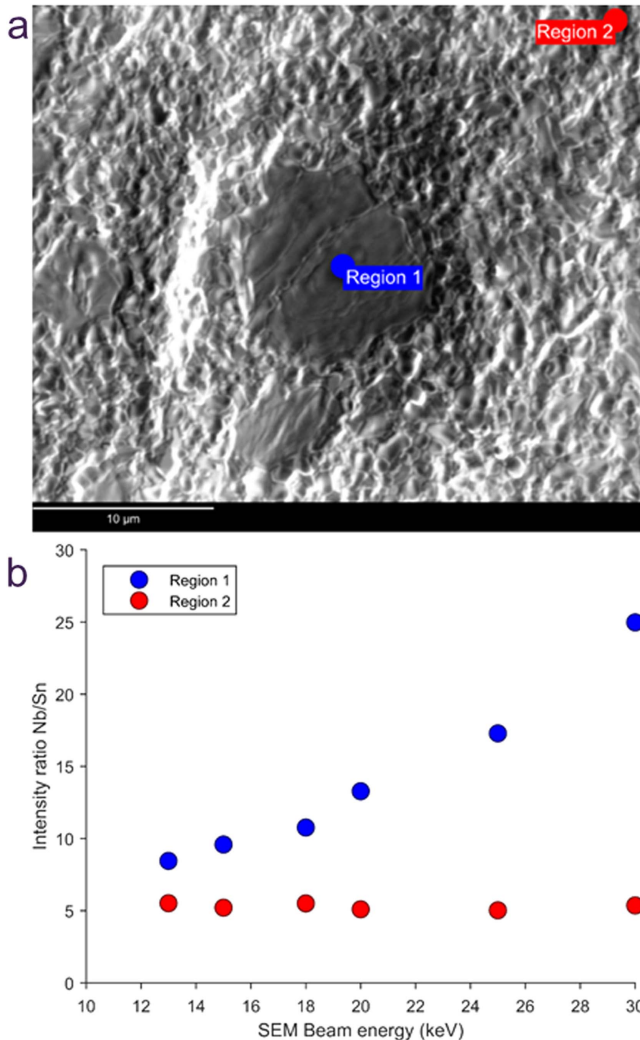


Figure 9. (a) SEM image of Nb₃Sn coating taken at Cornell University; (b) niobium to tin intensity in two regions of the surface versus SEM incident beam energy.

Nb₃Sn in the hot cutout is 5.290 ± 0.002 Å. According to previous measurements [13], lattice constants for both cutouts translate into Sn content in the desired range of 24–25 at%. WDS (figure 5) on cold cutout supports this assumption, Sn content of approximately 25 at% was obtained.

3.2. Microstructure

The SEM images in figures 6(a) and (b) demonstrate the surface of the coating in the cold and hot cutouts, respectively. The cold cutout is uniformly covered with micron-sized Nb₃Sn grains. The hot cutout, on the other hand, shows ‘patchy’ regions surrounded by the areas of uniform coating with an appearance similar to the cold cutout surface. EDS maps of the cold cutout measured with an incident accelerating electron voltage of 20 kV are highly uniform and completely featureless (not shown here), demonstrating lateral and in-depth uniformity for Sn and Nb. Sn content from EDS maps was estimated to 24–25 at%. Since Sn content

estimation from EDS agrees well with WDS measurements at the same accelerating voltage, as well as with XRD, we can conclude at an accelerating voltage of 20 kV, most of the EDS signal is coming from within the coating.

The appearance of the surface of the Nb₃Sn coating in the hot cutout is very different, compared to the cold one. Figure 7 shows an SEM image and corresponding Sn and Nb EDS maps of the hot cutout taken at an accelerating voltage of 20 kV. The patchy regions show significantly reduced Sn content (darker contrast in Sn map) and elevated Nb concentration (brighter contrast in Nb map). Reduced Sn signal in the EDS map can indicate either significantly reduced Sn concentration in the coating which no longer supports A15 structure or variation in thickness of the coating itself.

By varying the accelerating voltage of incident electrons in the SEM, one can change the probing depth for the EDS signal. Figure 8 demonstrates the result of changing the accelerating voltage. As we increase the incident electron voltage, the EDS probes a thicker surface layer. Most of the EDS signal comes from within the hot cutout’s coating at the lowest voltage of 10 kV, as can be seen from figure 8(a). Sn concentration measured in the 10 kV map, is close to 24 at%. Much lower Sn and higher Nb content observed in maps taken at 15 and 20 kV (figures 8(b) and (c), respectively) indicates that the EDS signal comes not only from the coating but also from the Nb underneath. Comparing figure 8(a) with figures 8(b) and (c), we can conclude that the Nb₃Sn coating in the patchy regions in the hot cutout is much thinner than in the cold one. The hot cutout shows significant variation in the Nb₃Sn coating thickness across the whole area.

Figure 9(a) shows an SEM picture of a typical patchy region taken at Cornell University. The ratio of the niobium to tin signal was measured by obtaining a point spectrum at the two locations shown in figure 9(a), at a number of different microscope beam energies. For each spectrum the ratio of the height of the Nb L_α₁ peak to the Sn L_α₁ peak is taken as an Nb/Sn intensity ratio, which is plotted as a function of the microscope beam energy in figure 9(b). The niobium-to-tin ratio in the patchy region (Region 1) increases with incident beam energy, since the contribution of niobium from the substrate increases. The niobium-to-tin ratio outside the patchy region (Region 2) remains constant with increasing beam energy, since the EDS interaction volume is concentrated within the thickness of the coating.

Cross-sectional TEM samples were prepared from the cold and hot cutouts to evaluate Nb₃Sn coating thickness directly. Figures 10(a) and (b) demonstrate TEM bright field (BF) images of the cold and hot cutouts, respectively. A FIB sample was taken from the patchy region of the hot sample, where SEM studies suggest that the coating is thinner. The difference in the Nb₃Sn coating thickness in the cold and hot cutouts is obvious when looking at TEM cross-sectional images. The Nb₃Sn coating is about 2 μm thick in the cold cutout and on the order of only 0.1 μm in the thinnest regions of the hot cutout. More than an order of magnitude difference in the Nb₃Sn thickness can be noticed comparing cold and hot cutouts.

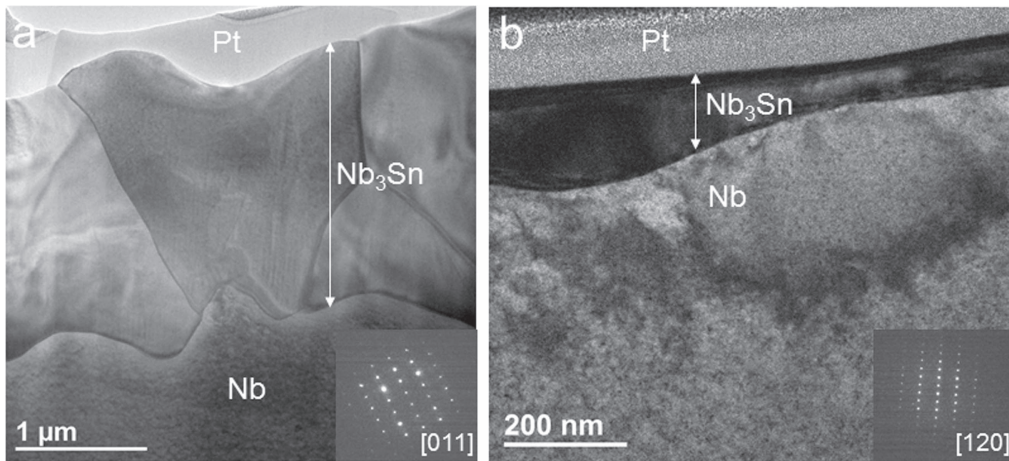


Figure 10. Bright Field image of FIB sample prepared from (a) cold and (b) hot cutouts with corresponding NED patterns taken from within Nb₃Sn grains.

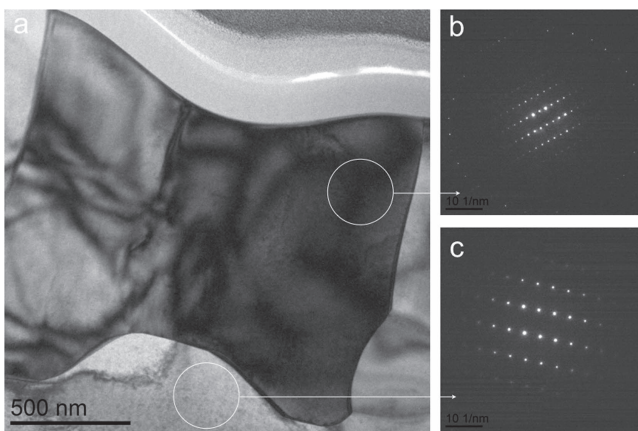


Figure 11. (a) BF image of Nb₃Sn coated sample's near-surface; (b) NED taken from within Nb₃Sn grain, [120] Nb₃Sn zone axis; (c) NED taken below the coating, Nb [113] zone axis.

It is worth mentioning that microstructure of the Nb₃Sn coating in the cold cutout is similar to the coating produced in the flat sample (figure 11).

The strong Q -slope observed in the ERL1-5 cavity could be explained by the presence of thin Nb₃Sn coating regions in the highly dissipating half-cell. A film thinner than the magnetic field penetration depth (about 100 nm for Nb₃Sn) may lead to currents in the Nb₃Sn–Nb interface and potentially into the Nb substrate. Our observations suggest that the poor Q -factors observed in RF tests of this cavity may largely be caused by dissipation in thin film areas that cover a large portion of the surface of one of the half-cells.

The microstructure of the coating is also different in the cold and hot cutouts. The coating in the cold cutout has approximately micrometer-sized Nb₃Sn grains compared to no visible grain boundaries in the TEM sample prepared from hot cutout. As it appears from EBSD taken from one of the patchy regions in the surface of hot cutout (figure 12), the entire thin (patchy) region is a single Nb₃Sn grain of about 100 μm in diameter. Our conclusions are supported by the analysis of five additional TEM samples prepared from cold cutout and two additional TEM

samples from hot cutout. Figure 10(a) shows contrast variation in the center of the largest grain which looks like a presence of some domain. The appearance of the intragrain domains in the cold cutout will be explored in the sections below.

In order to directly compare the thickness of the coating over an area much larger than the size of the TEM sample, small sections were saw cut from the hot and cold cutouts, and the cut surface was polished to create cross-sectional samples for SEM, as shown in figure 13. The sample from the hot spot demonstrates a rapidly changing, wavy Nb₃Sn/Nb interface which was not present in the original Nb substrate. The cause of this peculiar interface line will be investigated in future studies.

3.3. Origin of the thin coating

The thin Nb₃Sn (patchy) regions affect a significant area of the hot cutout but were not observed in the cold cutout. Hot and cold cutouts originate from two different cavity half-cells. The cause of the patchy regions may be attributed to the Nb substrate or the geometry of the deposition process (proximity of the Sn source) or both. In order to investigate potential causes, we explored two cutouts from the equator region of the cavity. In the equator cutouts, there is some representative area from both half-cells of the cavity on different sides of the weld. Most of the surface area in both equator cutouts show uniform Nb₃Sn coverage that looks identical to the coating in cold cutout. However, patchy regions of various sizes and shapes were found in random locations in either side of the weld (figure 14). EDS (figure 15) confirmed that the patchy regions in the equator cutouts are similar to the thin coating regions in the hot cutout. The surface area covered by the patchy regions and their size on the equator cutouts appear to be higher in the shiny half-cell compared to the matte half-cell. Though the mechanism of patchy regions formation is not clear, their presence in both half-cells of the coated cavity indicate that the deposition process may be more relevant than substrate-related issues. However additional studies would be beneficial to distinguish between these two possibilities and clearly pinpoint how these features grow.

A possible cause for the formation of patchy regions during the coating process is improper nucleation. Siemens

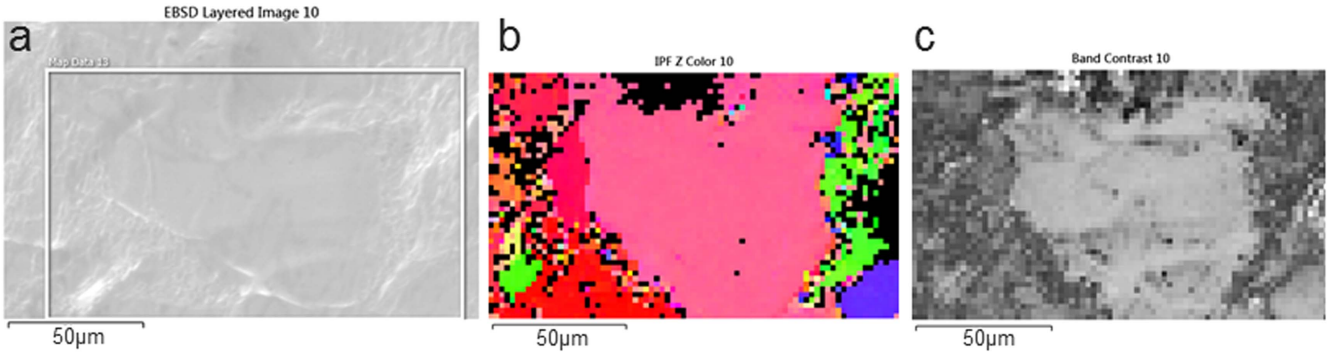


Figure 12. (a) SEM image of the patchy region on hot cutout surface; (b) inversed pole figures (IPF) colors; (c) band contrast.

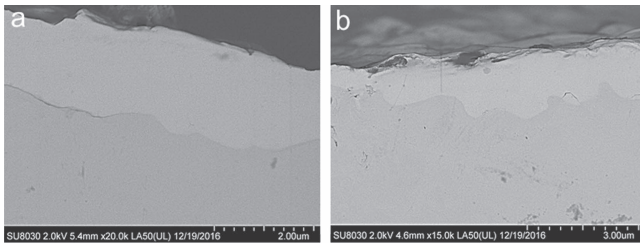


Figure 13. Backscattered images of cross-sectional SEM samples prepared from (a) cold cutout, (b) hot cutout.

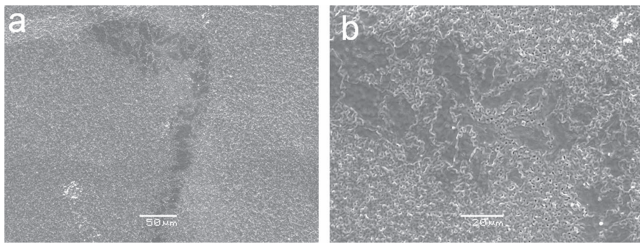


Figure 14. SEM image of the surface of equator spot (a) thin coating region, (b) detailed image of the thin region.

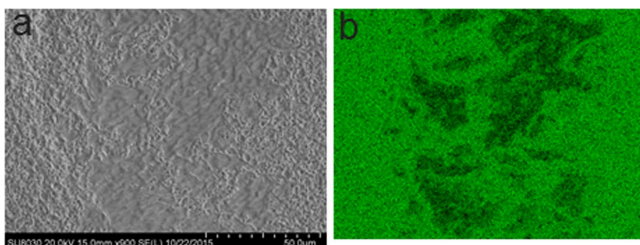


Figure 15. (a) SEM image of the equator cutout with corresponding (b) Sn map taken at 20 kV.

researchers showed that failure to perform a carefully controlled nucleation step could produce non-uniform regions of size $100\text{ }\mu\text{m}$ [14]. They describe two different nucleation methods: (1) anodizing the substrate prior to coating to generate a relatively thick niobium oxide, and, during initial heating, locally raising the temperature of the tin source to transport vapor to the surface while the temperature of the niobium substrate is still relatively low; (2) adding a small amount of SnF_2 , which has a relatively high vapor pressure at intermediate temperatures, well below the coating

temperature [14]. They explain that in experiments where they only partly anodize substrates, they observe a uniform coating in the anodized areas and incomplete coverage in the non-anodized areas [15]. They suggest that providing a high tin supply pressure to the substrate during early stages of the coating procedure allows a homogeneous nucleation layer to form prior to the niobium oxide dissolving and the tin coming into contact with the niobium surface [15].

This mechanism of the oxide acting as a buffer between the tin and the niobium until the nucleation layer is formed does not seem to be well explored experimentally. However, the non-uniformities observed in the past appear to be consistent with what is observed in the hot spot cutout. Furthermore, subsequent cavities coated at Cornell, which did not exhibit strong Q -slope or reduced low-field Q , received a modified recipe in which the tin source temperature was raised relative to that of the substrate during initial heating, as described in nucleation procedure (1) above. This may have helped to transport tin from the tin source to the substrate earlier, before the nucleation layer generated by the tin halide could fully diffuse into the surface (in the case of the Cornell cavities, SnCl_2 was used as a nucleation agent). Currently, this mechanism is largely speculative and much remains to be studied. For example, while Siemens has suggested that the thick oxide (generated by anodizing the substrate) improves Nb_3Sn coverage by acting as a buffer between the niobium and the tin, other explanations are quite possible, including a previously proposed catalytic effect of oxygen in the formation of Nb_3Sn [16].

3.4. Chemical characterization

Regardless of the coating thickness variation in the strongly dissipating half-cell, evaluation of the Nb_3Sn quality in the cavity is important for the development of this technology. Chemical characterization is vital since the superconducting properties of Nb_3Sn depend on stoichiometry. Small variations in Sn content can significantly impact superconducting properties of the coating. The Nb_3Sn A15 phase ranges from 18 at% to 26 at% of Sn [17]. A critical temperature of approximately 18 K can be reached only for ‘Sn-rich’ composition with approximately 24 at%–26 at% of Sn. In case of lower Sn content in the A15 phase, T_c can be as low as 6 K, below traditional Nb.

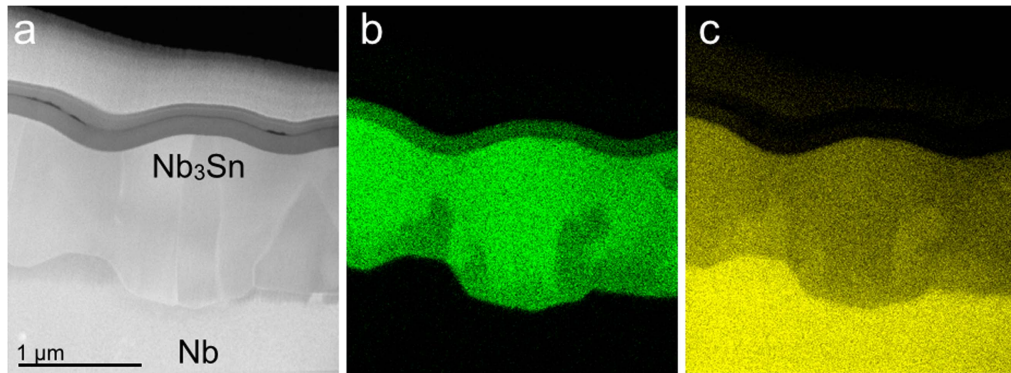


Figure 16. (a) Z-contrast image of the near-surface of the Nb₃Sn coated Nb sample; (b) EDS map for Sn; (c) EDS map for Nb.

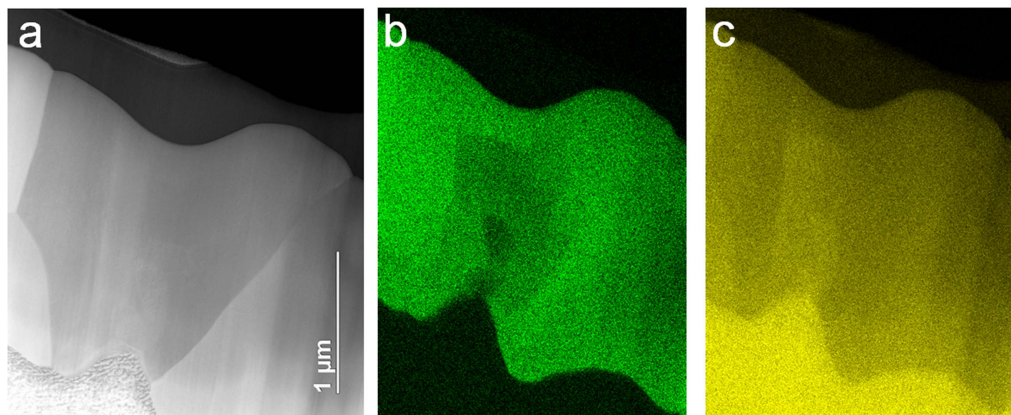


Figure 17. (a) Z-contrast image of the near-surface of cold cutout; (b) EDS map for Sn; (c) EDS map for Nb.

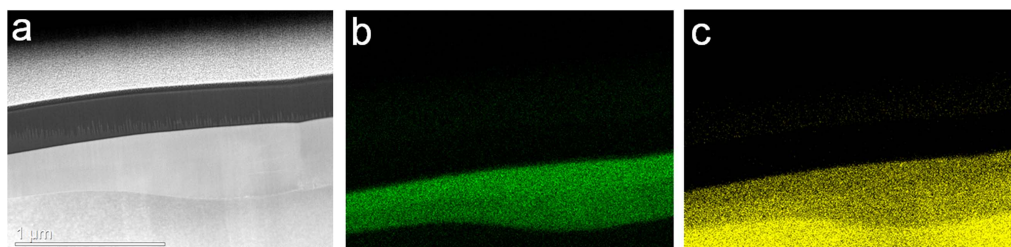


Figure 18. (a) Z-contrast image of the near-surface of hot cutout; (b) EDS map for Sn; (c) EDS map for Nb.

The presence of sub-micrometer-sized regions with locally reduced Sn concentration has previously been linked to a significant reduction of superconducting transition temperature in the Nb₃Sn coating. The effect of local compositional inhomogeneity on T_c for A15 compounds was first realized in the 1980s from specific heat and tunneling studies [18, 19]. In [20], tin-deficient regions within the Nb₃Sn film are reported in a witness sample coated with single cell cavity ERL1-4 which, as shown in figure 1, did not exhibit strong Q-slope, but did quench. There is no evidence that these regions are the cause of the quench degradation observed regularly between 14 and 17 MV m⁻¹ in Nb₃Sn cavities, but they are a candidate, based on the expected reduction in superconducting properties in these regions. It is therefore of interest to study these features. If the mechanism for their formation can be understood and suppressed, their effect on quench field could be studied.

The local composition of the Nb₃Sn coating in both the cutouts and the flat sample was explored with STEM/EDS mapping. Figure 16(a) shows a Z-contrast image of the flat sample's near-surface. EDS maps of Sn and Nb distribution in the near-surface are presented in figures 16(b) and (c), correspondingly. A Sn map of the near-surface shows several areas with decreased signal intensity in the Nb₃Sn coating. Areas with decreased Sn intensity are few hundred nm in size and are located close to the interface between Nb₃Sn and Nb. Decrease in the Sn signal intensity in the EDS map can be observed due to either a thinner region of the sample or a deficiency of Sn in this particular area. If thickness variation would be the cause, the Nb map would show the same areas of decreased Nb signal intensity. However, the Nb map shows brighter regions in Nb₃Sn coating, which indicates higher Nb content. Also, no obvious thickness variation can be observed

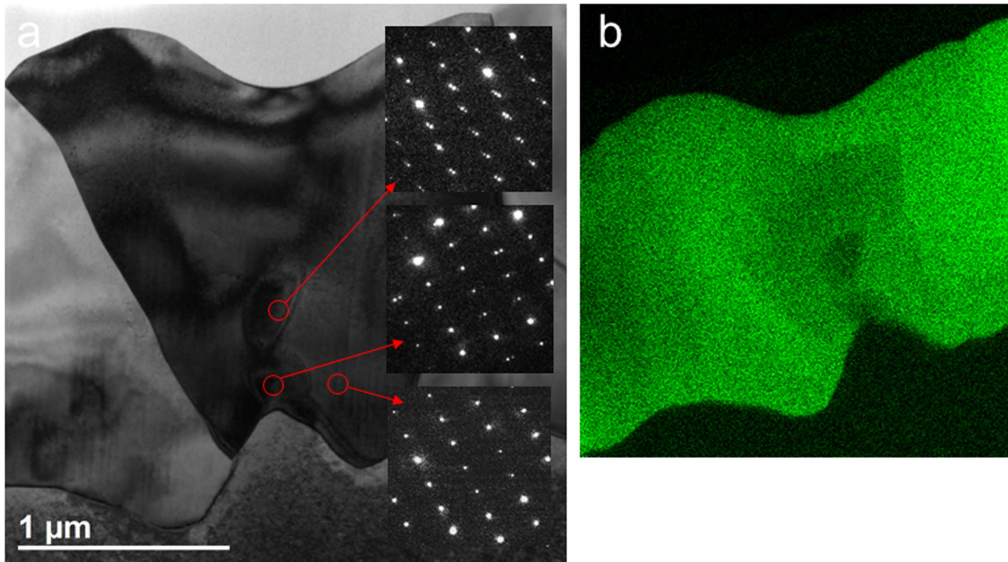


Figure 19. (a) BF TEM image of intragrain domain in cold cutout sample with NED patterns, (b) EDS Sn-map of the same area.

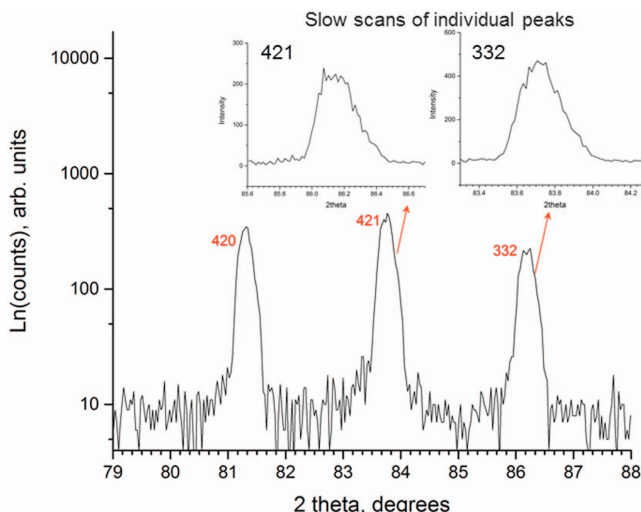


Figure 20. High-resolution slow XRD scan of cold cutout.

in corresponding STEM image of the area. Estimations of the Sn concentration difference between normal and Sn-deficient areas show a difference of 7–8 at%, regardless of the model used for EDS quantitative evaluation. Sn-deficiency do not mimic individual Nb₃Sn grains.

Sub-micrometer-sized regions of Sn-deficiency, similar to the ones observed in the flat sample's coating, were found in the Nb₃Sn coating in the cold cutout (figure 17). Three samples prepared from the cold cutout and one sample prepared from the flat sample were STEM/EDS measured. Sn-deficiency regions were found in all of them. The presence of Sn-deficiency regions in the flat sample implies that their formation is inherent to the deposition process rather than the substrate geometry. The appearance of a Sn-deficiency region approximately in the center of the largest grain in the cold cutout (figure 17) might be explained by a deficiency of Sn during grain growth. Sn from the surface is expected to diffuse along the grain boundaries during the deposition process [14, 21]. The region in the center

of the largest grain is the furthest from the grain boundaries which provide Sn source during the film growth.

Currently the questions of how much and what kind of performance degradation is induced by Sn-deficiency regions in Nb₃Sn cavities remain open. Since the temperature map of ERL1-5 was taken at fields less than 10 MV m⁻¹ due to rapidly degrading quality factor, the cold cutout does not show significant dissipation at such a low gradient. The Sn-deficiency regions most likely have reduced T_c [13], but they are also located close the Nb₃Sn/Nb interface. Being a few penetration depths away from the cavity surface, these Sn-deficiency regions would carry much less current compared to the surface. However, only a very small fraction of the cavity surface was observed in TEM cross sections; it is possible that there are also Sn-deficiency regions closer to the surface in other locations. Furthermore, quantitative estimation of the dissipation in Sn-deficiency regions is not trivial. The effect of local Sn-deficiency on the quality factor would need to be evaluated in a cavity free of thin coating regions which most likely cause severe Q -slope.

STEM/EDS characterization of hot cutout is demonstrated in figure 18. Two TEM samples prepared from a hot cutout were studied with the STEM/EDS. It was observed in both TEM samples that the Nb₃Sn coating in the hot cutout shows reduced Sn signal and brighter Nb signal at the bottom part of the coating. Observation of a lower Sn concentration at the bottom of the coating can be explained by insufficient Sn supply from the grain boundaries during the growth. Being a thin, 100 μm-sized single grain, the patchy region most likely demonstrates Sn-deficiency due to a lack of nearby grain boundaries to transport Sn below the surface. However, signal intensity variations in the Sn and Nb maps in the hot cutout samples are rather weak.

3.5. Characterization of Sn-deficiency regions in cold cutout

Sn-deficiency regions produce contrast variation in the TEM images in some samples (figure 19). Sn-deficiency regions look like domains in the largest Nb₃Sn grains in TEM and

Table 1. Summary of key results.

Method	Observation	Figure number
XRD	A15 Nb ₃ Sn structure, no spurious phases in cold and hot cutouts	Figure 4
SEM/ EDS	Uniform coating with 25 at% Sn and 75 at% Nb in cold cutout. Patchy, thin coating regions in hot and equator cutouts	Figure 6, figure 7, figure 9, figure 14, figure 15
TEM	Nb ₃ Sn coating in the hot cutout is more than an order of magnitude thinner than in cold cutout, as well as in flat Nb ₃ Sn-coated sample	Figure 10, figure 11
TEM/ EDS	Sn depleted regions with 7–8 at% deficiency of Sn in Nb ₃ Sn coating in cold cutout, as well as in Nb ₃ Sn-coated flat sample	Figure 17, figure 16
TEM/ NED	Sn depleted regions produce additional reflections in diffraction patterns. Sn depleted regions present as domains surrounded by Nb ₃ Sn with 25 at% Sn	Figure 19
EBSM	Patchy, thin regions in hot cutout are large grains with diameter of around 100 μm	Figure 12

TEM BF images. NED with a parallel beam of approximately 100 nm in diameter was used to explore the structure of Sn-deficient domains. Figures 19(a), (b) shows BF TEM image of intragrain domain in cold cutout sample and EDS Sn-map of the same area, respectively. Corresponding NED shows Nb₃Sn patterns from the intragrain Sn-deficient domain and the surrounding area from the same grain. No change in crystal structure within the grain containing the deficiency region was observed. However weak additional reflections accompany major diffraction spots inside the Sn-deficiency domain. Similar additional reflections were observed in intragrain domains in all cold cutout TEM samples.

The origin of the weak additional reflections in Sn-deficient domain is not yet understood. The challenge is that most of the observed additional reflections have low intensity under the imaging conditions that were used. One possible scenario can be realized from theoretical works of previous researchers [22]. Sn-deficiency regions in the Nb₃Sn A15 structure can be interpreted as accumulation of unit cells where missing Sn atoms are substituted by Nb atoms. The presence of Nb substitutions on Sn sites in some substantial volume potentially causes various crystal defects which were described in theoretical calculations. The possibility of anti-phase domains (like in Au–Cu alloys) can also be considered [23, 24].

The effect of compositional variation in Sn-deficiency regions on global properties of the film was explored with high-resolution XRD. One would expect a reduction of the lattice constant with lower Sn concentration. Since the A15 Nb₃Sn structure was already confirmed in the cold cutout, the shape of the diffraction peaks was investigated. Every Nb₃Sn diffraction peak in the cold cutout shows some asymmetry in the peak shape (figure 20). The asymmetry extends toward higher diffraction angles. According to Bragg's law, diffraction peaks at higher angles indicate smaller *d*-spacings in the diffracting material which, for cubic structures, translates into a smaller lattice constant. Previous experiments [13] show a decrease in *T_c* of Nb₃Sn with reduced lattice constant which was induced by lower Sn concentration. Consistent asymmetry of diffraction peaks shape indicates a spread in *d*-spacings in the diffracting material which can be interpreted as the presence of A15 Nb₃Sn with a few slightly different lattice constants. Smaller lattice constants most likely originate from the Sn-deficiency regions observed by STEM/EDS. The presence of a spread in lattice constants was previously reported in Nb₃Sn coating prepared by the same method [20].

Identical experimental conditions were used to explore diffraction peak shapes in hot cutout. However no asymmetry of the peaks was found in hot cutout which implies no spread in lattice constants values within available resolution.

4. Conclusion

For the first time, extended material characterization was carried out of Nb₃Sn-coated cavity cutouts with known dissipation profiles to correlate Nb₃Sn film features to degraded SRF performance. The key findings are summarized in table 1. Comparison of a 'hot' cavity cutout—with elevated surface

resistance which causes significant heating—to a 'cold cutout' revealed a significant difference in the Nb₃Sn coating thickness. A Nb₃Sn coating thickness under 100 nm was observed in the hot cutout. We suspect that insufficient coating thickness in the hot cutout enabled penetration of RF currents into the underlaying Nb and Nb₃Sn–Nb interface causing a substantial degradation of the cavity quality factor. In the hot cutout, Nb₃Sn grain diameter in the thin (patchy) regions approaches 100 μm. Formation of large, thin grains can be explained by insufficient Sn transport due to a low density of grain boundaries during the deposition process [15, 21].

Sub-micrometer-sized local composition variation regions were found in the minimally-dissipating cold cutout. The presence of Sn-deficiency regions in the cold cutout was directly observed with TEM imaging and STEM/EDS analysis in multiple TEM samples. Sn-deficiency effect on the lattice constant was measured with high-resolution XRD. For future work, extended material characterization of coupons from a Nb₃Sn-coated cavity without significant *Q*-slope would be beneficial to evaluate the severity of performance degradation due to local Sn-deficiency.

Acknowledgments

This work was carried out in part in the Frederick Seitz Material Research Laboratory Central Research Facilities, University of Illinois. The authors would like to thank all the staff scientists who work at Center for Microanalysis of Materials in Frederick Seitz Material Research Laboratory. This work made use of the EPIC, Keck-II, and/or SPID facility(ies) of Northwestern University's NUANCE Center, which has received support from the Soft and Hybrid Nanotechnology Experimental (SHyNE) Resource (NSF ECCS-1542205); the MRSEC program (NSF DMR-1121262) at the Materials Research Center; the International Institute for Nanotechnology (IIN); the Keck Foundation; and the State of Illinois, through the IIN.

Work performed at Cornell was primarily supported by US DOE award DE-SC0008431, and in part by the US National Science Foundation under Award PHY-1549132, the Center for Bright Beams. Select results presented in this work made use of the Cornell Center for Materials Research Shared Facilities which are supported through the NSF MRSEC program (DMR-1120296).

ORCID iDs

S Posen  <https://orcid.org/0000-0002-6499-306X>
J-M Zuo  <https://orcid.org/0000-0002-5151-3370>

References

- [1] Padamsee H 2009 *RF Superconductivity: Vol II: Science, Technology and Applications* (New York: Wiley-VCH)
- [2] Padamsee H S 2014 Superconductivity in high energy particle accelerators *Annu. Rev. Nucl. Part. Sci.* **64** 175

- [3] Transtrum M K, Catelani G and Sethna J P 2011 Superheating field of superconductors within Ginzburg–Landau theory *Phys. Rev. B* **83** 094505
- [4] Posen S, Liepe M and Hall D L 2015 Proof-of-principle demonstration of Nb₃Sn superconducting radiofrequency cavities for high Q_0 applications *Appl. Phys. Lett.* **106** 082601
- [5] Posen S and Liepe M 2014 Advances in development of Nb₃Sn superconducting radio-frequency cavities *Phys. Rev. ST Accel. Beams* **17** 112001
- [6] Müller G, Piel H, Pouryamout J, Boccard P and Kneisel P 2000 Nb₃Sn for RF applications *Workshop on Thin Film Coating Methods for Superconducting Accelerating Cavities (Hamburg)* ed D Proch TESLA Report 2000-15
- [7] Eremeev G, Reece C E, Kelley M J, Pudasaini U and Tuggle J R 2015 Progress with multi-cell Nb₃Sn cavity development linked with sample materials characterization *Proc. 17th Workshop on RF Superconductivity*
- [8] Posen S 2015 Understanding and overcoming limitation mechanisms in Nb₃Sn superconducting RF cavities *PhD Thesis* Cornell University
- [9] Posen S and Hall D L 2017 Nb₃Sn superconducting radiofrequency cavities: fabrication, results, properties, and prospects *Supercond. Sci. Technol.* **30** 033004
- [10] Posen S, Romanenko A, Merlo M and Trenikhina Y 2015 Fermilab Nb₃Sn cavity R&D program *Proc. 17th Workshop on RF Superconductivity*
- [11] Posen S, Liepe M and Hall D L 2015 Proof-of-principle demonstration of Nb₃Sn superconducting radiofrequency cavities for high Q_0 applications *Appl. Phys. Lett.* **106** 082601
- [12] Posen S, Romanenko A, Trenikhina Y, Melnychuk O and Sergatskov D A 2015 Cutout study of Nb₃Sn cavity *Proc. 17th Workshop on RF Superconductivity*
- [13] Godeke A 2006 A review of the properties of Nb₃Sn and their variation with A15 composition, morphology and strain state *Supercond. Sci. Technol.* **19** R68
- [14] Hillenbrand B 1980 The preparation of superconducting Nb₃Sn-surfaces for RF applications *Proc. SRF Workshop (Karlsruhe, Germany)*
- [15] Schnitzke K, Uzel Y, Hillenbrand B, Martens H and Pfister H 1977 Superconducting Nb₃Sn cavities with high microwave qualities *IEEE Trans. Magn.* **MAG-13** 491–5
- [16] Braginski A I, Gavaler J R and Schulze K 1986 *Formation of A15 Phase in Epitaxial and Polycrystalline Nb-Sn Diffusion Couples* (Boston, MA: Springer) pp 585–92
- [17] Devantay H, Jorda J L, Decroux M and Muller J 1981 The physical and structural properties of superconducting A15-type Nb–Sn alloys *J. Mater. Sci.* **16** 2145–53
- [18] Hellman F and Geballe T H 1987 Specific heat of thin-film a15 superconductors: an anomalous inhomogeneity discovered *Phys. Rev. B* **36** 107–20
- [19] Talvacchio J, Hellman F, Marshall A F and Geballe T H 1986 A new look at the growth of thin films of Nb–Sn *Adv. Cryog. Eng. Mater.* **32** 593
- [20] Becker C, Posen S, Groll N, Cook R, Schleptz C M, Hall D L, Liepe M, Pellin M, Zasadzinski J and Proslier T 2015 Analysis of Nb₃Sn surface layers for superconducting radio frequency cavity applications *Appl. Phys. Lett.* **106** 082602
- [21] Farrell H H, Gilmer G H and Suenaga M 1974 Grain boundary diffusion and growth of intermetallic layers: Nb₃Sn *J. Appl. Phys.* **45** 4025–35
- [22] Dienes G J, Welch D O and Lazareth O W Jr 1984 Defects and diffusion mechanisms in Nb₃Sn *J. Phys. Chem. Solids* **45** 1225–42
- [23] Marcinkowski M J and Zwell L 1963 Transmission electron microscopy study of the off-stoichiometric Cu₃Au superlattices *Acta Metall.* **11** 390
- [24] Zhu J and Cowley J M 1982 Microdiffraction from antiphase domain boundaries in Cu₃Au *Acta Crystallogr. A* **38** 718–24